A Design Proposal of Silicon-on-Insulator Mach-Zehnder Interferometers

Christos Tsokos

***Abstract*— This report presents the design of a strip-waveguide Mach–Zehnder interferometer (MZI) for silicon-on-insulator (SOI) fabrication. The device is analyzed using a combination of analytical models and numerical simulations to quantify key performance metrics, including phase response, interference behavior, and transmission characteristics. The results are used to justify the chosen design parameters and to provide insight into the trade-offs that govern SOI MZI performance.**

***Index Terms*— Silicon Photonics, Mach-Zehnder interferometer**

I. INTRODUCTION

Silicon-on-insulator (SOI) photonics has become a leading integrated photonics platform because it enables high-index-contrast waveguides, compact passive devices, and compatibility with CMOS fabrication [1] [2]. Among the fundamental building blocks in SOI is the Mach–Zehnder interferometer (MZI), which converts optical phase differences into measurable intensity variations through interference. MZIs are widely used for optical modulation, switching, sensing, filtering, and characterization of waveguide phase and loss [3][5].

In an SOI MZI, light from an input waveguide is split into two arms, accumulates a relative phase delay due to differences in effective index and/or path length, and is then recombined at a second coupler. The resulting transmission depends on the phase difference $\Delta\phi$, which is wavelength-dependent through the propagation constant $\beta(\lambda) = 2\pi n_{eff}(\lambda)/\lambda$. Accurate modeling therefore requires capturing both the waveguide dispersion (variation of n_{eff} with wavelength) and practical non-idealities such as propagation loss and imperfect splitting ratios. For imbalanced MZIs, these effects produce spectral fringes with a free spectral range (FSR) that is governed by the arm length difference and the waveguide group index.

This report presents the modeling of an SOI Mach–Zehnder interferometer using a compact waveguide model and an analytical interferometer transfer function. The simulation predicts the optical transmission spectrum around 1550 nm, and key performance metrics such as spectral variation across a wavelength sweep, and sensitivity to design parameters (arm length difference). The results provide both physical insight into MZI behavior on SOI and practical guidance for designing broadband splitters and interferometric devices in silicon photonic circuits.

C. Tsokos is with the Photonic Communications Research Laboratory at the National Technical University of Athens, Zografou 15573, Athens, Greece (ctso@mail.ntua.gr).

II. THEORY

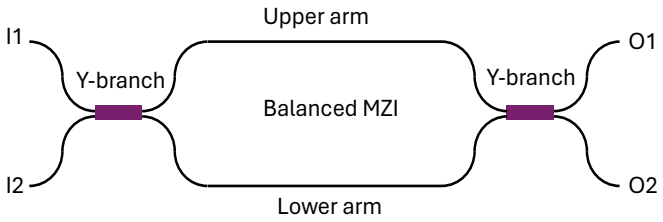

Fig. 1 Functional layout of a balanced MZI.

We consider the balanced Mach–Zehnder interferometer shown in Fig. 1, implemented with two ideal 3-dB Y-branches acting as a splitter and a combiner. Let the complex input fields at the two input ports be E_{I1} and E_{I2}. An ideal 3-dB Y-branch splitter launches equal-amplitude fields into the two arms; using a symmetric representation, the fields at the entrance of the upper and lower arms can be written as:

$$E_{u,l}(0) = \frac{E_{I1} + E_{I2}}{\sqrt{2}} \tag{1}$$

The fields then propagate through the upper and lower arms of lengths, L_u and L_l, accumulating phase according to the waveguide propagation constant:

$$\beta(\lambda) = \frac{2 \cdot \pi \cdot n_{eff}(\lambda)}{\lambda} \tag{2}$$

Neglecting any additional phase-shifting element, the fields at the input of the output Y-branch are:

$$E_u(L_u) = E_u(0) \cdot e^{-i\beta_u L_u - \frac{a_u}{2}L_u} \tag{3}$$

$$E_l(L_l) = E_l(0) \cdot e^{-i\beta_l L_l - \frac{a_l}{2}L_l} \tag{4}$$

, where a_u and a_l the propagation loss experienced into the two arms. Assuming that only input 1 is active ($E_{O2} = 0$) and neglect any propagation loss ($a_u = a_l = 0$), at the output port of the second Y-branch, the fields are:

$$E_{O1,2} = \frac{E_u(L_u) + E_l(L_l)}{\sqrt{2}} \tag{5}$$

$$E_{O1,2} = \frac{1}{2} \cdot E_{I1}(e^{-i\beta_u L_u} + e^{-i\beta_l L_l}) \tag{6}$$

As the light intensity is proportional to the squared power of the field amplitude, the light intensity at the output of the MZI can

be written as:

$$I_{O1,2} = \frac{1}{4} \cdot |E_{I1}(e^{-i\beta_u L_u} + e^{-i\beta_l L_l})|^2 \quad (7)$$

Given that both interferometer arms use the same waveguide geometry and no additional optical phase shifter is included, the propagation constant are equal:

$$\beta_u = \beta_l = \frac{2 \cdot \pi \cdot n_{eff,u}(\lambda)}{\lambda} = \frac{2 \cdot \pi \cdot n_{eff,l}(\lambda)}{\lambda} = \beta \quad (8)$$

In this way, eq. (7) is simplified to:

$$I_{O1,2} = \frac{1}{2} \cdot I_{I1} \cdot (1 + \cos(\beta \Delta L)) \quad (9)$$

, where $I_{I1} = E_{I1}^2$ and $\Delta L = L_u - L_L$.

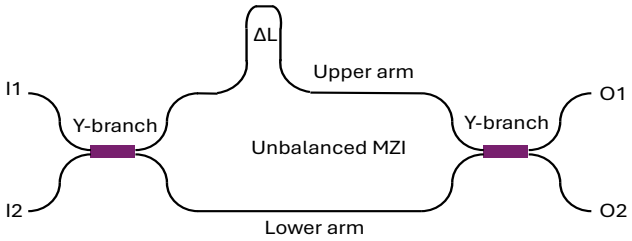

Fig. 2 Functional layout of an unbalanced MZI.

Fig. 2 shows the functional layout of an MZI in which the two arms have different optical path lengths ($L_u \neq L_L$), so the relative phase between the two propagated fields becomes strongly wavelength-dependent. When the fields recombine at the output coupler, this varying phase produces alternating constructive and destructive interference, resulting in a sinusoidal transmission spectrum with periodic maxima and minima; the spacing of these fringes is the free spectral range (FSR):

$$FSR(\lambda) = \frac{\lambda^2}{\Delta L \cdot n_g(\lambda)} \quad (10)$$

, where n_g is the group index defined as:

$$n_g(\lambda) = n_{eff}(\lambda) - \lambda \frac{dn_{eff}(\lambda)}{d\lambda} \quad (11)$$

III. Modelling and Simulation

For the simulation studies, the standard strip-waveguide geometries was considered. Table 1 summarizes the silicon core dimension (width and height) together with the surrounding silicon-dioxide cladding thickness. For completeness and reproducibility, the key finite-difference eigenmode (FDE) solver settings used in the analysis are also listed.

Table 1 Simulated waveguide geometries.

Obj.	Geometry Param.	Design 1
Si	Width span (nm)	500
	Height span (nm)	220
SiO2	Width span (nm)	4
	Height span (nm)	4
FDE solver	Width span (nm)	2.5
	Height span (nm)	2
	Mesh cells x	100
	Mesh cells y	100

A. Strip waveguide with 500 nm width

The following section presents the characteristics of waveguide geometry.

Table 2 Effective, group indices and loss for TE1 and TM1

λ =1500 nm	Neff	Group index
TE1	2.506654	4.197804
TM1	1.837414	4.021323

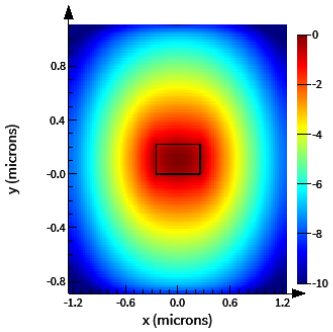

Fig. 3 Field intensity of TE1.

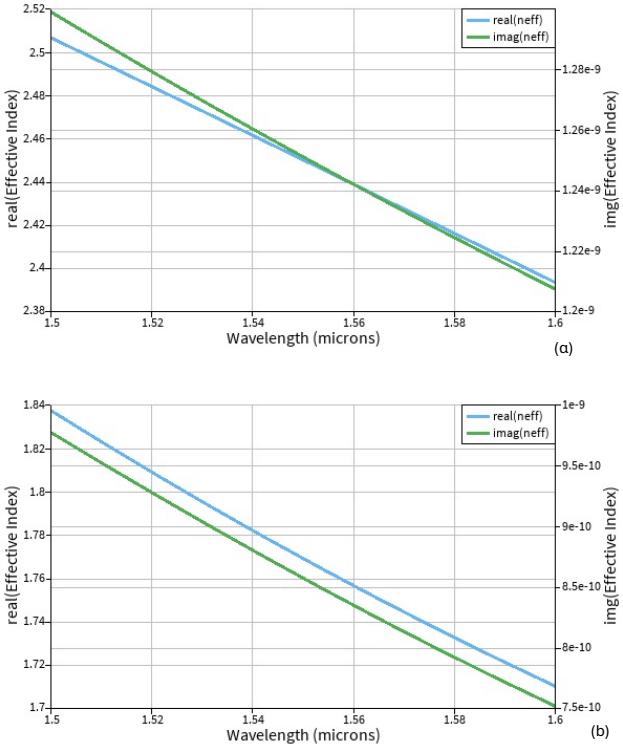

Fig. 4 Effective indices over wavelength for TE1 and TM1.

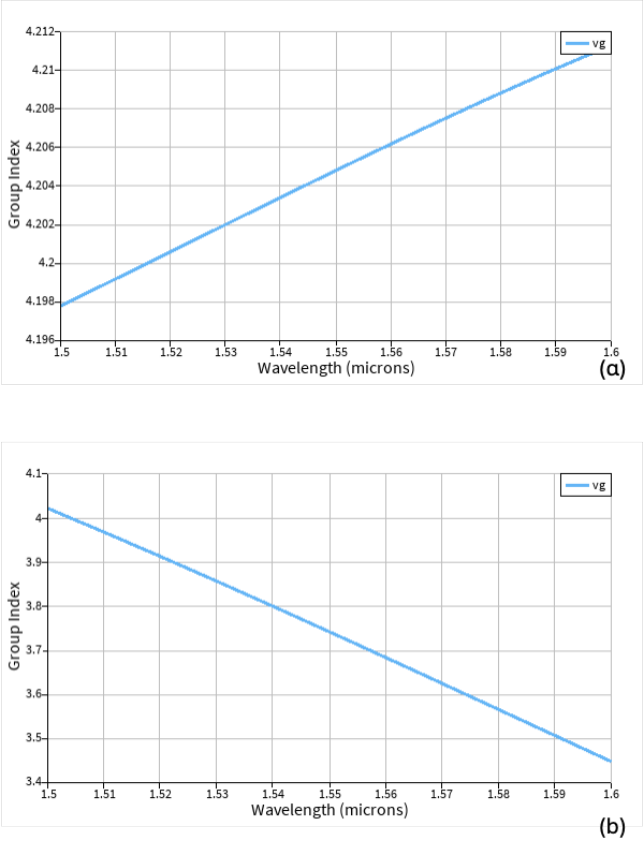

Fig. 5 Group indices over wavelength for TE1 and TM1.

The compact models of this waveguide geometry for TE1 and TM1 modes are:

$$n_{eff,TE1}(\lambda) = 2.45017 - 1.13197 \cdot (\lambda - \lambda_0) - 0.0441148 \cdot (\lambda - \lambda_0)^2 \quad (12)$$

$$n_{eff,TM1}(\lambda) = 1.76917 - 1.27212 \cdot (\lambda - \lambda_0) + 1.86092 \cdot (\lambda - \lambda_0)^2 \quad (13)$$

B. Mach-Zehnder Interferometer designs

For the design of the unbalanced MZIs, we select to work with the TE mode of the three waveguide geometries. Table 3 presents the simulated FSRs for length asymmetries 0 μm, 25 μm, 50 μm, 75 μm and 100 μm.

Table 3 Simulated FSR of unbalanced MZI based for λ = 1500 nm on the three selected waveguide geometries.

ΔL (μm)	**FSR (nm)**
0	No fringes
30	17.87
50	10.72
70	7.66
90	5.96
110	4.87
130	4.12

Fig 6 presents the simulation setup developed for the purposes of the current report emulating a MZI.

Fig. 7 and Fig 8 depict the transfer function of the grating couplers and Y-branched, respectively. As expected, both devices are wavelength-dependent show a strong attenuation as we move away from the central wavelength of 1550 nm.

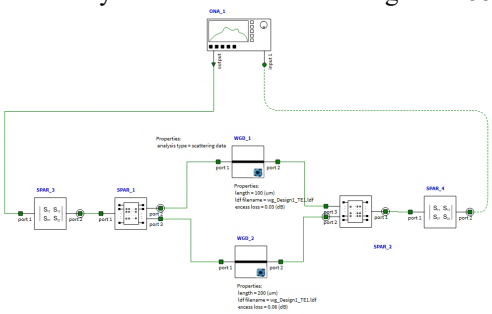

Fig. 6 Simulation setup in Interconnect.

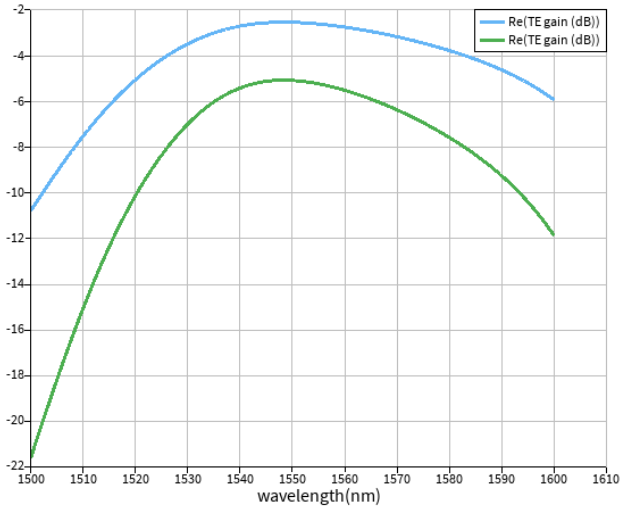

Fig. 7 Transfer function of a single (blue) and dual (green) GCs.

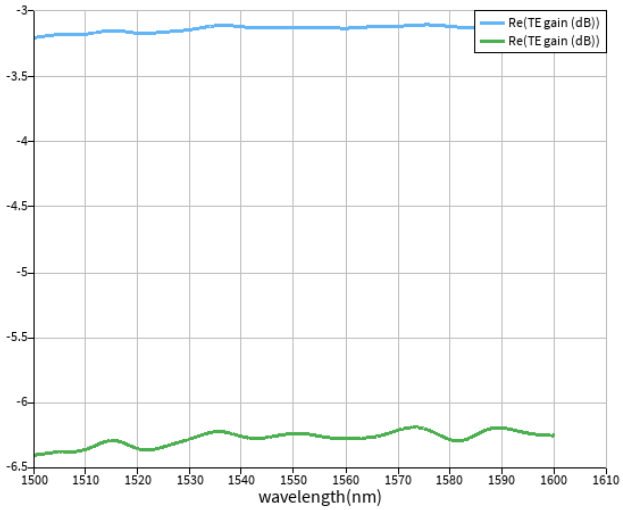

Fig. 8 Transfer function of a single (blue) and dual (green) Y-branches.

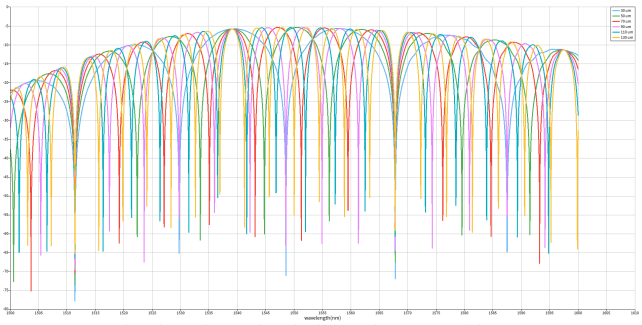

Fig. 9 Transfer function of unbalanced MZIs with 25 um, 50 um, 75 um and 100 um length asymmetry using Design-1 waveguide geometry.

Finally, Fig 9 presents the transfer function of the simulated and designed unbalanced MZIs from 1500 nm to 1600 nm.

V. Conclusion

References

[1] Bogaerts, Wim, and Lukas Chrostowski. "Silicon photonics circuit design: methods, tools and challenges." Laser & Photonics Reviews 12.4 (2018): 1700237.

[2] Siew, Shawn Yohanes, et al. "Review of silicon photonics technology and platform development." Journal of Lightwave Technology 39.13 (2021): 4374-4389.

[3] Dhote, Chandresh, Anamika Singh, and Santosh Kumar. "Silicon photonics sensors for biophotonic applications—a review." IEEE Sensors Journal 22.19 (2022): 18228-18239.

[4] Chen, Lawrence R. "Silicon photonics for microwave photonics applications." Journal of Lightwave Technology 35.4 (2017): 824-835.

[5] Yamada, Koji, et al. "High-performance silicon photonics technology for telecommunications applications." Science and Technology of Advanced Materials 15.2 (2014): 024603.